Self-Assembly of Novel Mesoporous Manganese Oxide Nanostructures and Their Application in Oxidative Decomposition of Formaldehyde

Hongmin Chen,[†,§] Junhui He,[*,†] Changbin Zhang,[‡] and Hong He[‡]

Functional Nanomaterials Laboratory and Key Laboratory of Organic Optoelectronic Functional Materials and Molecular Engineering, Technical Institute of Physics and Chemistry, Chinese Academy of Sciences (CAS), Beijing 100080, P.R. China, Graduate University of Chinese Academy of Sciences, Beijing 100049, P.R. China, and State Key Laboratory of Environmental Chemistry and Ecotoxicology, Research Center for Eco-Environmental Sciences, Chinese Academy of Sciences (CAS), Beijing 100085, P.R. China

Received: July 31, 2007; In Final Form: September 18, 2007

Monodisperse manganese oxide honeycomb and hollow nanospheres have been prepared facilely at room temperature by varying the molar ratio of $KMnO_4$ and oleic acid. These new nanomaterials were characterized by XRD, SEM, EDS, TEM, and BET measurements. They had robust nanostructures and were stable even after ultrasonic treatment (40 kHz, 120 W) for 30 min. A plausible mechanism of the formation of manganese oxide nanostructures was proposed. The manganese oxide nanomaterials showed high catalytic activities for oxidative decomposition of formaldehyde at low temperatures. Complete conversion of formaldehyde to CO_2 and H_2O could be achieved, and harmful byproducts were not detected in effluent gases. The catalytic activity of manganese oxide hollow nanospheres was much higher than that of honeycomb nanospheres, although the surface area of the latter was nearly 2 times as high as that of the former. The mechanism of such morphology-dependent catalytic activity was discussed in detail. The catalytic activities of the obtained manganese oxide nanospheres were also significantly higher than those of previously reported manganese oxide octahedral molecular sieve (OMS-2) nanorods, MnO_x powders, and alumina-supported manganese-palladium oxide catalysts. Potential applications and future research efforts were proposed.

1. Introduction

Controlling the size, shape, and structure of inorganic nanomaterials to search for new properties has become one of the major objectives of nanoscale science and technology, because of their structure-, size-, and shape-dependent characteristics and novel electronic, magnetic, optical, chemical, and mechanical properties that cannot be obtained in their bulk counterparts.[1,2] Oxides of transition metals, which have different oxidation states and coordination numbers, are especially interesting due to their unique electronic, optical, thermal, photonic, and catalytic properties in different morphologies.[3] Recently, much attention has been paid to 3D nanostructures, such as TiO_2, SnO_2, MnO_2, and Fe_2O_3 hollow spheres and other nanostructures.[4] Among various strategies for controlled synthesis, the "soft chemistry" route, which is based on a solution process, is effective for the synthesis of nanostructured materials with well-controlled shapes, sizes, and structures.[5]

Manganese oxides (MnO_2) have been extensively studied as a well-known transition-metal oxide, because of their outstanding structural multiformity combined with novel chemical and physical properties and wide applications in catalysis, ion or molecular sieves, molecular adsorption, biosensors, electrode materials in batteries, and energy storage.[6−14] Different MnO_2 morphologies have so far been prepared, including rods, wires, tubes, urchin-like microstructures, etc. They were prepared either by oxidizing Mn^{2+} with oxidants or by reducing MnO_4^- with reductants. Very recently, Suib and co-workers[15] prepared cryptomelane-type MnO_2 octahedral molecular sieve microspheres (OMS-2) and mesoporous γ-MnO_2 hollow nanospheres by hydrothermal method. Xie and co-workers[16] prepared β-MnO_2 nanorods, urchin-like α-MnO_2 microspheres and α-MnO_2 hierarchical structures via a homogeneous catalytic route. However, few works were reported on nanostructures of layered MnO_2, such as birnessite-type MnO_2 (A_xMnO_2, where $A = H^+$ or metal cation). A_xMnO_2 is a layered structure consisting of edge-sharing MnO_6 octahedra with an interlayer spacing of ca. 0.7 nm.[17] It can be widely used in applications, such as ionic adsorption,[18] battery electrodes,[19] electrochemical and magnetic materials,[20,21] and oxidative degradation of organic and inorganic contaminations.[22] Hydrothermal reaction,[23] sol−gel process,[24] reflux method,[25] and thermal decomposition[26] have been used to synthesize MnO_2 materials of various ordered morphologies. Obtained MnO_2 particles, however, were several microns in size and most of the prepared methods needed catalysts, acid or alkaline media, or high temperatures.

Formaldehyde is a major indoor air pollutant and is known to cause irritation to eyes, respiratory tract, and skin even at concentrations of ppm levels.[27] It exists in isolating materials, furniture, wood, exhaust gases, disinfectants, and tobacco smoke. It is also used as an additive in water-based paints. Currently effective removal of HCHO is attracting much attention. The catalytic decomposition of HCHO has been achieved in the temperature range 90∼500 °C. Facile decomposition of HCHO at low temperature, however, is still a challenge though there are increasing concerns on HCHO in the indoor environment.

* To whom correspondence should be addressed. Tel.: +86-10-8254 3535. Fax: +86-10-8254 3535. E-mail: jhhe@mail.ipc.ac.cn.

† Technical Institute of Physics and Chemistry, Chinese Academy of Sciences.

‡ Research Center for Eco-Environmental Sciences, Chinese Academy of Sciences.

§ Graduate University of Chinese Academy of Sciences.

10.1021/jp076113n CCC: $37.00
Published on Web 11/15/2007

CHART 1: Synthetic Procedures of K_xMnO_2 Honeycomb and Hollow Nanospheres (C_{KMnO4} = Concentration of $KMnO_4$).

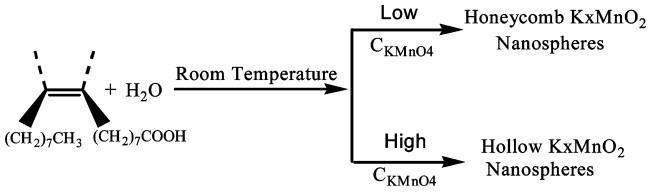

Catalytic oxidation is a promising approach as HCHO can be oxidized to CO_2 over catalysts at lower temperatures than thermal oxidation.[28] MnO_x powders, MnO_2 octahedral molecular sieve (OMS-2) nanorods, and alumina-supported manganese-palladium oxides ($Mn-Pd/Al_2O_3$) were used as catalysts for decomposition of HCHO, and the latter two catalysts showed high activities at low temperatures.[29] Very recently, Sinha et al.[30] reported that mesostructured 2.8 wt % Au/γ-MnO_2 nanoparticle composites could be used for extensive air purification.

In this article, we reported self-assembly of manganese oxide nanoplatelets into novel mesoporous nanostructures and their application in oxidative decomposition of formaldehyde. Complete conversion of HCHO to CO_2 and H_2O was achieved at low temperatures, and harmful byproducts were not detected in effluent gases. The as-prepared mesoporous nanostructures also showed better catalytic activities for decomposion of HCHO than other existing MnO_2 materials.

2. Experiments

K_xMnO_2 honeycomb nanospheres and hollow nanospheres were synthesized via a simple soft chemistry route at room temperature, as described in Chart 1.Oleic acid (OA) was oxidized by potassium permanganate ($KMnO_4$) in neutral aqueous solution. Such a reaction was also called "Baeyer test for unsaturation".[31]

2.1. Materials. Potassium permanganate (≥99.5%), oleic acid (≥99.5%), and ethanol (≥99.7%) were purchased from Beijing Chemical Reagent Company and used without further purification. Distilled water was used throughout.

2.2. Synthesis of K_xMnO_2 Honeycomb Nanosphere. In a typical procedure, 1.0 g (6.3 mmol) of $KMnO_4$ was dissolved in 500 mL of distilled water, and the mixture was fleetly stirred for about 30 min. A total of 10.0 mL of oleic acid was added, and a steady emulsion was formed. After the emulsion was maintained at room temperature for a certain period of time, brown−black products were collected and washed several times with distilled water and alcohol to remove any possible residual reactants. Finally, the products were dried under a vacuum at 60 °C for 10 h.

2.3. Synthesis of K_xMnO_2 Hollow Nanospheres. A total of 2.0∼4.0 g (12.6∼25.2 mmol) of $KMnO_4$ was dissolved in 200 mL of distilled water, and the mixture was stirred for about 30 min. A total of 4.0 mL of oleic acid was added, and a steady emulsion was formed. After the emulsion was maintained at room temperature for a certain period of time, brown−black products were collected and washed several times with distilled water and alcohol to remove any possible residual reactants. Finally, the products were dried under a vacuum at 60 °C for 10 h.

2.4. Oxidative Decomposition of Formaldehyde on K_xMnO_2 Nanomaterials. Catalytic activities of as-prepared samples for the oxidation of HCHO were studied with a fixed-bed quartz flow reactor (length = 300 mm, diameter = 4 mm) by passing a gas mixture of 100 ppm HCHO, 20 vol % O_2, and the balance gas (He) at a total flow rate of 50 cm^3 min^{-1} in a space velocity of GHSV = 50 000 h^{-1}.[32] A total of 50∼70 mg of catalysts were loaded. HCHO, CO, and CO_2 were analyzed on-line using a gas chromatograph (GC) equipped with hydrogen flame ionization detector (FID) and Ni catalyst converter which was used for converting carbon oxides and HCHO quantitatively into methane in the presence of hydrogen before the detector. Separation of reactants and products was achieved using two columns: a carbon molecular sieve column for permanent gases (CO and CO_2) and a GDX-403 column for HCHO. The HCHO conversion was determined by the equation

$$\text{HCHO conversion (\%)} = \frac{[\text{HCHO}]_b - [\text{HCHO}]}{[\text{HCHO}]_b} \times 100 \quad (1)$$

where $[HCHO]_b$ (ppm) is the HCHO concentration without passing over catalyst, [HCHO] (ppm) is the HCHO concentration after passing over catalyst.

2.5. Characterization. Powder X-ray diffraction (XRD) patterns of as-prepared samples were recorded on a Holand PANalytical X'Pert PRO MPD X-ray diffractometer with Cu Kα radiation (λ = 0.1542 nm) operated at 40 kV and 40 mA. The 2θ range and recording step were 10∼90° and 0.03°, respectively. Crystallite sizes were calaulated using the Scherrer equation. For the crystallite size calculation, the (001) reflection of as-synthesized K_xMnO_2 at a 2θ of 12.29° was used. Scanning electron microscopy (SEM) and energy dispersive spectroscopy (EDS) measurements were carried out on a Hitachi S-4300 field emission scanning electron microscope (FESEM). All of the samples were sputtered with gold before observation. For transmission electron microscopy (TEM), powder samples were added on the carbon-coated copper grids and observed on a JEOL JEM-200CX transmission electron microscope at an acceleration voltage of 150 kV. Nitrogen adsorption−desorption measurements were performed on a Quantachrome NOVA 4200e surface area analyzer (measurable diameter range 0.35∼200 nm) at −196 °C using the volumetric method. The as-prepared K_xMnO_2 products were first dried at 150 °C before analysis. The specific surface area was calculated by the Brunauer−Emmett−Teller (BET) method using a linear plot over the range P/P_0 = 0.04∼0.20 (six points collected). Pore size distributions were estimated from the adsorption branch of the isotherm by the Barrett, Joyner, and Halenda (BJH) method. Pore volumes were determined from the amount of nitrogen adsorbed at P/P_0 = 0.98.

3. Results and Discussion

3.1. Crystalline Structures and Elemental Analyses. The phase and crystallographic structure of the products were determined by XRD. Figure 1, panels a and b, shows XRD patterns of honeycomb and hollow nanospheres, respectively. They have similar patterns. Significant XRD peaks recorded at 2θ = 12.29, 24.33, 36.60, and 65.67° could be well assigned to the (001), (002), (100), and (110) planes of K_xMnO_2 with a turbostratic structure.[33] The d-spacings of these planes were estimated to be 0.718 nm (001), 0.366 nm (002), 0.246 nm (100), and 0.142 nm (110). The increase in intensity of the (100) peak was probably related to scattering from remaining organics. From 2θ = 12.29°, the interlayer spacing was estimated to be ca. 0.72 nm, in good agreement with the literature.[17,33] For the particle size estimation, the (001) reflection at 2θ = 12.29° was used. Calculation by the Scherrer equation showed that the lamellar structure of K_xMnO_2 had a thickness of ca. 8.1 nm.

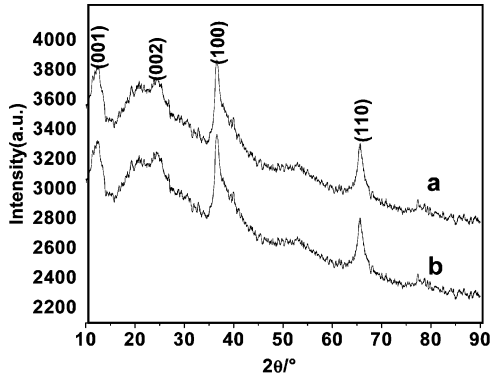

Figure 1. XRD patterns of as-prepared honeycomb (a) and hollow (b) K_xMnO_2 nanospheres, respectively.

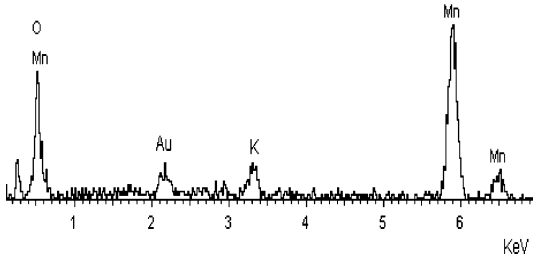

Figure 2. EDS analysis of as-prepared K_xMnO_2 nanospheres.

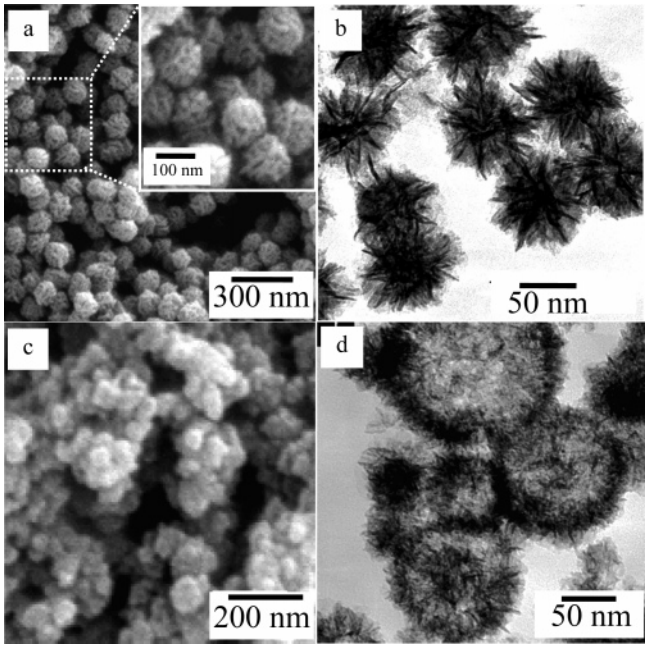

Figure 3. SEM (a) and TEM (b) images of honeycomb K_xMnO_2 nanospheres ($KMnO_4$/OA = 1:5) and SEM (c) and TEM (d) images of hollow K_xMnO_2 nanospheres ($KMnO_4$/OA = 1:1).

Thus, it is supposed to consist of ca. 7 monolayers. The corresponding EDS results (Figure 2) confirmed the presence of Mn, O, and K elements and gave rough atomic ratios of Mn/O and K/Mn of 1:2 and 0.05, respectively. K_xMnO_2 of $x < 0.3$ was also reported previously.[21]

3.2. Morphologies of K_xMnO_2 Nanospheres. Figure 3a shows a typical SEM image of the product obtained using a $KMnO_4$/OA molar ratio of 1:5 after redox reaction for 20 h. Clearly, the product consists of monodisperse nanospheres of ca. 97 nm in diameter. A magnified image (inset of Figure 3a) shows that the nanosphere in fact has a honeycomb structure that was formed by the self-assembly of nanoplatelets.[15] The thickness of such platelets was estimated to be ca. 10.7 nm, in agreement with the above XRD results. Figure 3b shows a typical TEM image of the honeycomb nanospheres. Clearly, each nanosphere consists of platelets that self-align perpendicular to the spherical surface and emanate from the center rather like the structure of a honeycomb.[15,34] Gray parts are platelets that were vertical to the electron beam, and dark parts are those that were parallel to the electron beam. Figure 3, panels c and d, shows SEM and TEM images, respectively, of the product obtained using a molar ratio of $KMnO_4$/OA at 1:1 after redox reaction for 5 h. The clear contrast between the dark edge and the gray center of each nanosphere (Figure 3d) is evidence of its hollow nature.[35] A close look at the shells shows that they consist of shorter and thinner platelets than the above honeycomb K_xMnO_2 nanospheres. Their size distribution is also not as uniform as that of the latter. It is very interesting that both the honeycomb and hollow K_xMnO_2 nanospheres had no changes in morphology upon ultrasonic treatment (40 kHz, 120 W) for 30 min, indicating the robustness of the nanospheres. The validity of the above synthetic approaches on a larger scale was also confirmed by increasing the precursor quantities by 10 fold.

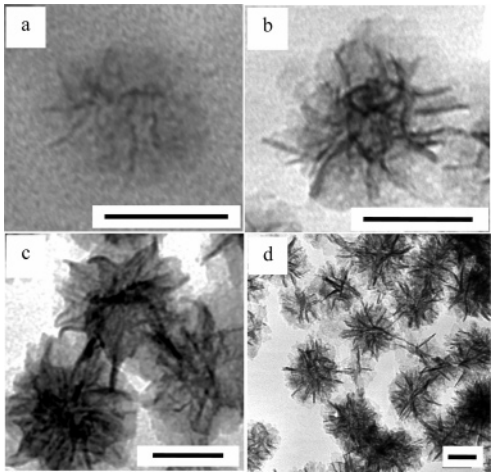

Figure 4. TEM images of honeycomb $KxMnO_2$ nanospheres obtained after redox times of 0.5 (a), 2 (b), 5 (c), and 20 h (d), respectively. Scale bar: 50 nm.

3.3. Evolution of Honeycomb K_xMnO_2 Nanospheres with Reaction Time. The size and morphology evolution of honeycomb K_xMnO_2 nanospheres were investigated by varying the reaction time. After 0.5 h of redox reaction, the color of the solution had little changes, and only a small amount of solid was obtained. As shown in Figure 4a, the nanostructure (ca. 50 nm in size) consisted of nanoplatelets of ca. 2.2 nm in thickness. The contrast was low, probably because of a small number of nanoplatelets. After 2 h, the color of the solution changed from purple−red to yellow−brown, showing that more K_xMnO_2 was formed. As shown in Figure 4b, clear sphere-like nanostructures were formed, in which nanoplatelets self-assembled by standing on each other. The nanostructure and the nanoplatelets were 75 nm in size and 3.0 nm in thickness, respectively. With further increase of reaction time, the color of the solution gradually changed to brown−black, and the size of the nanostructure and the thickness of the nanoplatelet increased to nearly 83 and 3.3 nm (5 h, Figure 4c), 89 and 5.2 nm (20 h, Figure 4d), respectively. Clearly, the nanoplatelets eventually self-aligned perpendicular to the spherical surface and emanate from the center rather like the structure of a honeycomb (Figure 4d).[36] Thus, the thickness of the platelet and the size and morphology of nanospheres are dependent on the redox reaction time.[37] Another interesting observation was that the lamellar platelets

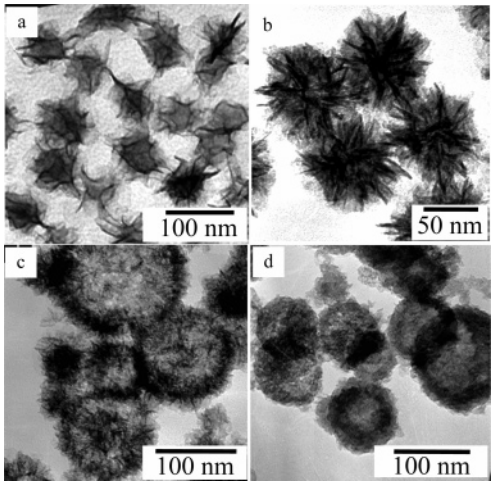

Figure 5. TEM images of K_xMnO_2 nanostructures obtained with molar ratios of $KMnO_4$/OA of 1:10 (a), 1:5 (b), 1:1 (c), and 2:1 (d), respectively.

initially looked very soft and foldable. In fact, such softness has recently been discussed on the nanometer scale in a review article.[38]

3.4. Effect of the Molar Ratio of $KMnO_4$/OA on the Size and Morphology of K_xMnO_2 Nanospheres. The effect of the molar ratio of $KMnO_4$/OA on the size and morphology of K_x-MnO_2 nanospheres was also studied. Figure 5a shows a TEM image of product obtained with a $KMnO_4$/OA molar ratio of 1:10. Irregular sphere-like nanostructures with soft and foldable lamellar nanoplatelets were obtained. They were similar in morphology to those nanostructures in Figure 4, panels b and c, which had also been observed in other crystal phases of MnO_2.[39] At a higher $KMnO_4$/OA molar ratio of 1:5, honeycomb nanpspheres were obtained, as shown in Figure 5b. Very interesting, hollow nanospheres were produced at a still higher $KMnO_4$/OA molar ratio of 1:1(Figure 5c). Their shells consisted of loosely packed nanoplatelets and had a thickness of ca. 20 nm. When the molar ratio of $KMnO_4$/OA further increased to 2:1, hollow nanospheres of denser shells were obtained (Figure 5d). Therefore, the size and morphology of K_xMnO_2 nanospheres are largely dependent on the molar ratio of $KMnO_4$/OA, and it is possible to tailor the K_xMnO_2 nanostructures by adjusting this parameter.

3.5. Formation Mechanism of the Nanostructures. In principle, crystal growth and crystal morphology are determined by the degree of supersaturation, the species to the surface of the crystals, the surface and interfacial energies, and the structure of the crystals. Various extrinsic and intrinsic factors, the crystal structure, and the growth surroundings are accounted for in the final morphology.[40]

Based on the above analysis, a plausible mechanism was proposed and is shown in Scheme 1. Oleic acid can form a stable O/W emulsion at appropriate concentrations (process a).[41] In the emulsion, the "Baeyer test for unsaturation" reaction quickly occurs between $KMnO_4$ and oleic acid at the O/W interface and produces K_xMnO_2 nuclei there (process b).[42] At low $KMnO_4$ concentrations, small amounts of lamellar K_xMnO_2 platelets are produced, and thus an unstable shell of loosely packed platelets is formed (process c). Removal of oleic acid and formed cis-diol by ethanol results in collapse of the shell, giving honeycomb nanospheres (process d). In contrast, large amounts of lamellar platelets are produced at high $KMnO_4$ concentrations, and thus a robust shell of densely packed platelets is formed (process e). Therefore, the K_xMnO_2 shell is

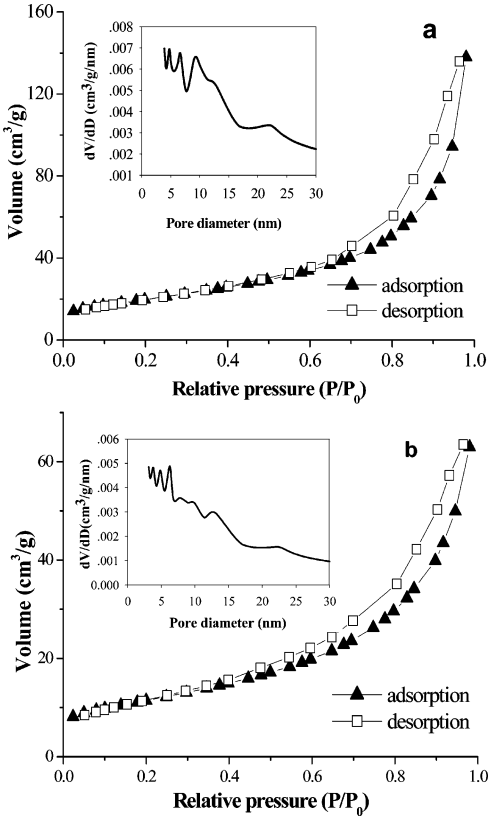

Figure 6. Nitrogen sorption isotherms and pore size distributions (inset) of honeycomb (a) and hollow (b) K_xMnO_2 nanospheres.

SCHEME 1: Plausible Formation Mechanism of Honeycomb and Hollow K_xMnO_2 Nanospheres

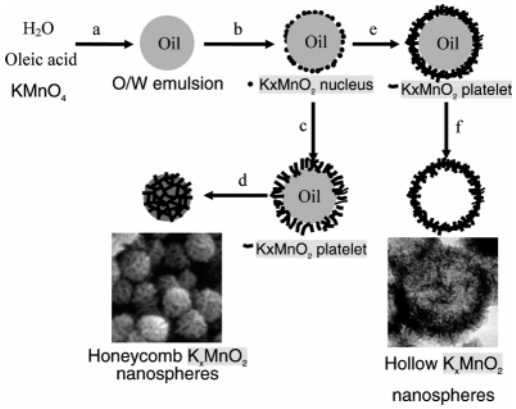

preserved even after removal of oleic acid and formed cis-diol, and hollow nanospheres are formed (process f). Thus, the current approach is believed to be a general method for preparation of metal oxide hollow nanospheres.

3.6. Nitrogen Adsorption−Desorption Measurements. The surface area and pore size distribution of the above nanomaterials were revealed by N_2 adsorption−desorption measurements. The results showed that both the honeycomb and hollow nanospheres had a typical type IV adsorption−desorption isotherm with a hysteresis loop characteristic of mesoporous materials based on the IUPAC (Figure 6).[43] The BET surface areas of the honeycomb and hollow nanospheres were calculated to be 70.70 and 40.69 m^2/g, respectively. The corresponding pore volumes are 0.20 and 0.09 cm^3/g, respectively. As shown by BJH analyses, the pore size of the honeycomb nanosphere has a tri-modal distribution at 4.9, 6.5, and 9.0 nm (Figure 6a, inset), and that of the hollow nanosphere has a multi-modal

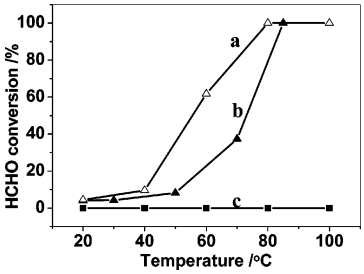

Figure 7. HCHO conversion on control (■), honeycomb K_xMnO_2 nanospheres (70 mg) (▲), and hollow K_xMnO_2 nanospheres (50 mg) (△), respectively.

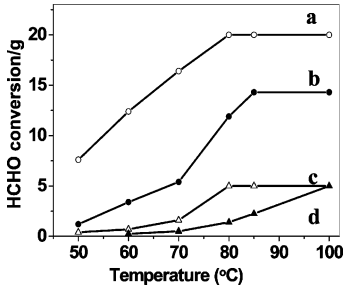

Figure 8. HCHO conversion per gram of samples on MnO_x powder (▲), OMS-2 nanorods (△), honeycomb (●) and hollow (○) K_xMnO_2 nanospheres, respectively.

distribution at 3.7, 4.7, 6.2, and 13.0 nm (Figure 6b, inset), respectively. The mesopores are attributed to the interstitial space between nanoplatelets of honeycomb and hollow nanostructures. These results agree well with those of XRD, SEM, and TEM measurements. The high BET surface area is beneficial as catalyst or catalyst supports for catalytic reactions.

3.7. Oxidative Decomposition of Formaldehyde on As-Synthesized K_xMnO_2 Nanospheres. A sample (50 mg) of the hollow K_xMnO_2 nanospheres showed the highest catalytic activity for decomposition of HCHO, and at 60 °C, the HCHO conversion reached 61.8% (Figure 7, curve a). A sample (70 mg) of the honeycomb nanospheres achieved a HCHO conversion of 24% at the same temperature (Figure 7, curve b). The HCHO conversion by the hollow K_xMnO_2 nanospheres (50 mg) increased to 100% when the temperature was raised to 80 °C, and that by the honeycomb nanospheres (70 mg) needed 85 °C to reach a 100% conversion. In sharp contrast, no HCHO conversion was noticeable in a control experiment. This is the first report of catalytic decomposition of HCHO by mesoporous layered K_xMnO_2 nanomaterials at such low temperatures.

The catalytic activities of the as-prepared K_xMnO_2 nanomaterials were compared with those of previous reported materials. OMS-2 nanorods (200 mg) showed a HCHO conversion of 13% at 60 °C. It increased to 100% when the reaction temperature was raised to 80 °C.[29] Mn 18.2 wt %/Al_2O_3 catalysts (100 mg) had no activity at temperatures lower than 150 °C. The HCHO conversation by these catalysts reached 100% when reaction temperature was increased to 220 °C. Mn 18.2 wt %/Pd 0.4 wt %/Al_2O_3 catalysts (100 mg) gave a HCHO conversation of 100% at temperatures higher than 80 °C.[29] Both OMS-2 nanorods (200 mg) and Mn 18.2 wt %/Pd 0.4 wt %/Al_2O_3 (100 mg) catalysts had no catalytic activity when reaction temperature was lower than 50 °C.[29] Even though the mesoporous hollow K_xMnO_2 nanospheres had a surface area nearly 2 times lower than that of mesoporous honeycomb K_xMnO_2 nanospheres, it still showed a much higher catalytic activity for the HCHO conversion. The HCHO conversion per gram of the hollow K_xMnO_2 nanospheres (Figure 8, curve a) is about 4 times as high as that of the honeycomb K_xMnO_2 nanospheres (Figure 8, curve b) at 60 °C and about 2 times as high as that of the honeycomb K_xMnO_2 nanospheres at 80 °C. In contrast, OMS-2 nanorods and MnO_x powders gave a HCHO conversion per gram of less than 1 at 60 °C (Figure 8, curve c) and of less than 5 at 80 °C (Figure 8, curve d). Thus, the catalytic activities of these MnO_2 nanomaterials for HCHO oxidation fall in the order of hollow K_xMnO_2 nanospheres > honeycomb K_xMnO_2 nanospheres > OMS-2 nanorods > MnO_x powders. Clearly, the catalytic activity of MnO_2 nanomaterial is largely dependent on its morphology. The hollow K_xMnO_2 nanospheres would adsorb and retain HCHO for a longer period of time than the honeycomb K_xMnO_2 nanospheres and eventually enhance the oxidation of HCHO. The smaller size of nanoplatelets in hollow K_xMnO_2 nanospheres than in honeycomb K_xMnO_2 nanospheres would be another reason for their higher catalytic activity.

4. Conclusion

In summary, we developed a facile approach to preparation of mesoporous nanospheres of layered MnO_2 at room temperature. It involves a redox reaction of $KMnO_4$ and oleic acid at the O/W interface, followed by self-assembly of formed K_xMnO_2 nanoplatelets into K_xMnO_2 nanostructures. Both monodisperse honeycomb and hollow K_xMnO_2 nanospheres were prepared in high yields depending on the molar ratio of $KMnO_4$/OA. These new nanomaterials had robust nanostructures and showed morphology-dependent catalytic activities for decomposition of formaldehyde. Complete conversion of HCHO to CO_2 and H_2O could be achieved at low temperatures, and harmful byproducts were not detected in effluent gases. The catalytic activities were also significantly higher than those of previously reported MnO_2 OMS-2 nanorods, MnO_x powders, and Mn−Pd/Al_2O_3 catalysts. Although TiO_2 had no activity for HCHO oxidation, TiO_2-supported noble metals (Pt, Au, Pd, and Rh) showed high activities under otherwise identical conditions when the noble metal loading reached a certain quantity.[32] Palladium also enhanced the activity of 18.2 wt %Mn/Al_2O_3 catalysts, as discussed above.[28,29] Thus, the mesoprous K_xMnO_2 nanospheres would be convenient and effective catalysts and catalyst supports for noble metals, such as Pt, Au, Pd, and Rh.[32,44] In fact, they are currently being investigated as catalyst supports for noble metal nanaparticles in our laboratory. Such materials are also believed to have applications as adsorbents and separation materials,[18] and in electrodes, electrolytes,[19] and electromagnetic and electronic devices.[20]

Acknowledgment. We are grateful to the "Hundred Talents Program" of CAS, the National Basic Research Program of China (Grant No. 2006CB933000), and the National Natural Science Foundation of China (Grant No.20471065) for financial supports.

References and Notes

(1) (a) Hu, J. T.; Odom, T. W.; Lieber, C. M. *Acc. Chem. Res.* **1999**, *32*, 435. (b) Hupp, J. T.; Poeppelmeier, K. R. *Science* **2005**, *309*, 2008.

(2) (a) Huang, M. H.; Mao, S.; Feick, H.; Yan, H.; Wu, Y.; Kind, H.; Weber, E.; Russo, R.; Yang, P. *Science* **2001**, *292*, 1897. (b) Chen, J.; Xu, L. N.; Li, W. Y.; Gou, X. L. *Adv. Mater.* **2005**, *17*, 582.

(3) (a) Tian, Z.; Tong, W.; Wang, W. J.; Duan, N.; Krishnan, V. V.; Suib, S. L. *Science* **1997**, *276*, 926. (b) Toberer, E. S.; Seshadri, R. *Adv. Mater.* **2005**, *17*, 2244.

(4) (a) Chen, H.; He, J. *Chem. Lett.* **2007**, *36*, 174. (b) Mao, Y. B.; Kanungo, M.; Benny, T. H.; Wong, S. S.; *J. Phys. Chem. B* **2006**, *110*, 702. (c) Lou, X. W.; Wang, Y.; Yuan, C. L.; Lee, J. Y.; Archer, L. A. *Adv. Mater.* **2006**, *18*, 2325. (d) Li, X. H.; Zhang, D. H.; Chen, J. S. *J. Am. Chem. Soc.* **2006**, *128*, 8382. (e) Wang, S. T.; Feng, L.; Jiang, L. *Adv.*

Mater. **2006**, *18*, 767. (f) Caruso, F.; Spasova, M.; Susha, A.; Giersig, M.; Caruso, R. A. *Chem. Mater.* **2001**, *13*, 109.
(5) Cushing, B. L.; Kolesnichenko, V. L.; O'Connor, C. J. *Chem. Rev.* **2004**, *104*, 3893.
(6) (a) Thackeray, M. M. *Prog. Solid State Chem.***1997**, *25*, 1. (b) Espinal L, Suib S L and Rusling J F. *J. Am. Chem. Soc.* **2004**, *126*, 7676.
(7) Armstrong, A. R.; Bruce, P. G. *Nature* **1996**, *381*, 499.
(8) Ammundsen, B.; Paulsen, J. *Adv. Mater.* **2001**, *13*, 943.
(9) Winter, M.; Brodd, R. J. *Chem. Rev.* **2004**, *104*, 4245.
(10) Toupin, M.; Brousse, T.; Bélanger, D. *Chem. Mater.* **2002**, *14*, 3946.
(11) Cheng, F. Y.; Zhao, J.; Song, W.; Li, C.; Ma, H.; Chen, J.; Shen, P. *Inorg. Chem.* **2006**, *45*, 2038.
(12) Wills, A. S.; Raju, N. P.; Greedan, J. E. *Chem. Mater.* **1999**, *11*, 1510.
(13) (a) Segal, S. R.; Park, S. H.; Suib, S. L. *Chem. Mater.* **1997**, *9*, 98. (b) Greedan, J. E.; Raju, N. P.; Wills, A. S.; Morin, C.; Shaw, S. M. *Chem. Mater.* **1998**, *10*, 3058.
(14) Yamamoto, S.; Matsuoka, O.; Fukada, I.; Ashida, Y.; Honda. T.; Yamamotoy, N. *J. Catal.* **1996**, *159*, 401.
(15) (a) Yuan, J. K.; Li, W. N.; Gomez, S.; Suib, S. L. *J. Am. Chem. Soc.* **2005**, *127*, 14184. (b) Yuan, J.; Laubernds, K.; Zhang, Q.; Suib, S. L. *J. Am. Chem. Soc.* **2003**, *125*, 4966.
(16) Li, Z. Q.; Ding, Y.; Xiong, Y. J.; Yang, Q.; Xie, Y. *Chem. Commun.* **2005**, 918.
(17) (a) Ma, Y.; Luo, J.; Suib, S. L. *Chem. Mater.* **1999**, *11*, 1972. (b) Feng, Q.; Kanoh, H.; Ooi, K. *J. Mater. Chem.* **1999**, *9*, 319. (c) Golden, D. C.; Chen, C. C.; Dixon, J. B. *Clays Clay Miner.* **1987**, *35*, 271.
(18) Lina, A. A.; Dyer, A.; Harjula, R. *J. Mater. Chem.* **2003**, *13*, 2963.
(19) Aronson, B. J.; Kinser, A. K.; Passerini, S.; Smyrl, W. H.; Stein, A. *Chem. Mater.* **1999**, *11*, 949.
(20) Nakayama, M.; Konishi, S.; Tagashira, H.; Ogura, K. *Langmuir* **2005**, *21*, 354.
(21) (a) Mori, S.; Chen, C. H.; Cheonq, S. W. *Nature* **1998**, *392*, 473. (b) Ge, J.; Zhuo, L.; Yang, F.; Tang, B.; Wu, L. Z.; Tung, C. *J. Phys. Chem. B* **2006**, *110*, 17854.
(22) (a) Ahn, M.; Fillry, T. R.; Jafvert, C. T.; Nies, L.; Hua, I.; Cruz, J. *Environ. Sci. Technol.* **2006**, *40*, 215. (b) Barrett, K. A.; Mcbride, M. B. *Environ. Sci. Technol.* **2005**, *39*, 9223. (c) Sekine, Y. *Atmos. Environ.* **2002**, *36*, 5543.
(23) Gaillot, A. C.; Lanson, B.; Drits, V. A. *Chem. Mater.* **2005**, *17*, 2959.
(24) Ching, S.; Roark, J. L.; Duan, N.; Suib, S. L. *Chem. Mater.* **1997**, *9*, 750.
(25) Yang, X.; Tang, W.; Feng, Q.; Ooi, K. *Cryst. Growth Des.* **2003**, *3*, 409.
(26) Omomo, Y.; Sasaki, T.; Wang, L.; Watanabe, M. *J. Am. Chem. Soc.* **2003**, *125*, 3568.
(27) Collins, J. J.; Ness, R.; Tyl, R. W.; Krivanek, N.; Esmen, N. A.; Hall, T. A. *Regul. Toxicol. Pharm.* **2001**, *34*, 17.
(28) (a) Álvarez-Galván, M. C.; de la Peña O'Shea, V. A.; Fierro, J. L. G.; Arias, P. L. *Catal. Commun.* **2003**, *4*, 223. (b) Imamura, S.; Uchihori, D.; Utani, K. *Catal. Lett.* **2004**, *24*, 377.
(29) (a) Tang, X. F.; Huang, X. M.; Shao, J. J.; Liu, J. L.; Li, Y. G.; Xu, Y. D.; Shen, W. J. *Chin. J. Catal.* **2006**, *27*, 97. (b) Álvarez-Galván, M. C.; Pawelec, B.; de la Peña, O'Shea, V. A.; Fierro, J. L. G.; Arias, P. L. *Appl. Catal. B: Environ.* **2004**, *51*, 83.
(30) Sinha, A. K.; Suzuki, K.; Takahara, M.; Azuma, H.; Nonaka, T.; Fukumoto, K. *Angew. Chem., Int. Ed.* **2007**, *46*, 2891.
(31) Fessenden, R. J.; Fessenden, J. S. *Organic Chemistry*; Willard Grant Press: Boston, MA, 1979; p 413.
(32) (a) Zhang, C.; He, H.; Tanaka, K. *Catal. Commun.* **2005**, *6*, 211. (b) Zhang, C.; He, H.; Tanaka, K. *Appl. Catal. B: Environ.* **2006**, *65*, 37.
(33) (a) Villalobos, M.; Lanson, B.; Manceau, A.; Toner, B.; Sposito, G. *Am. Miner.* **2006**, *91*, 489. (b) Drits, V. A.; Silvester, E.; Gorshov, A. I.; Manceau, A. *Am. Miner.* **1997**, *82*, 946.
(34) (a) Zhong, L.; Hu, J.; Liang, H.; Cao, A.; Song, W.; Wan, L. *Adv. Mater.* **2006**, *18*, 2426. (b) Liu, B.; Zeng, H. C. *J. Am. Chem. Soc.* **2004**, *126*, 8124.
(35) Caruso, F.; Caruso, R. A.; Möhwald, H. *Science* **1998**, *282*, 1111.
(36) (a) Wang, D.; Song, C.; Hu, Z.; Fu, X. *J. Phys. Chem. B* **2005**, *109*, 1125. (b) Cao, A.; Hu, J.; Liang, H.; Wan, L. *Angew. Chem., Int. Ed.* **2005**, *44*, 4391.
(37) Lameiras, F. S. *Mater. Res.* **1999**, *2*, 139.
(38) He, J.; Kunitake, T. *Soft Matter* **2006**, *2*, 119.
(39) Wu, C.; Xie, Y.; Wang, D.; Yang, J.; Li, T. *J. Phys. Chem. B* **2006**, *107*, 13583.
(40) Wang, X. L.; Yan, C. L.; Zou, L. J.; Xue, D. F. *Inter. J. Nanosci.* **2006**, *5*, 219.
(41) Cheng, X.; Liu, S.; Lu, L.; Sui, X.; Meynen, V.; Cool, P.; Vansant, E. F.; Jiang, J. *Microporous Mesoporous Mater.* **2006**, *98*, 41.
(42) Huang, J.; Xie, Y.; Li, B.; Liu, Y.; Qian, Y.; Zhang, S. *Adv. Mater.* **2000**, *12*, 808.
(43) Sing, K. S. W.; Everett, D. H.; Haul, R. A. W.; Moscou, L.; Piertti, R. A.; Rouquèrol, J.; Siemieniewska, T. *Pure Appl. Chem.* **1985**, *57*, 603.
(44) Cellier, C.; Ruaux, V.; Lahousse, C.; Grange, P.; Gaigneaux, E. M. *Catal. Today* **2006**, *117*, 350.